How reduced excitonic coupling enhances light harvesting in the main photosynthetic antennae of diatoms

Tjaart P. J. Krüger[a,1], Pavel Malý[b,c], Maxime T. A. Alexandre[b], Tomáš Mančal[c], Claudia Büchel[d], and Rienk van Grondelle[a,b]

[a]Department of Physics, University of Pretoria, Hatfield 0028, South Africa; [b]Department of Physics and Astronomy, Vrije Universiteit Amsterdam, 1081 HV Amsterdam, The Netherlands; [c]Faculty of Mathematics and Physics, Charles University, 121 16 Prague 2, Czech Republic; and [d]Institute of Molecular Biosciences, Department of Biosciences, Goethe University Frankfurt, 60438 Frankfurt, Germany

Edited by Krishna K. Niyogi, Howard Hughes Medical Institute, University of California, Berkeley, CA, and approved November 13, 2017 (received for review August 23, 2017)

Strong excitonic interactions are a key design strategy in photosynthetic light harvesting, expanding the spectral cross-section for light absorption and creating considerably faster and more robust excitation energy transfer. These molecular excitons are a direct result of exceptionally densely packed pigments in photosynthetic proteins. The main light-harvesting complexes of diatoms, known as fucoxanthin–chlorophyll proteins (FCPs), are an exception, displaying surprisingly weak excitonic coupling between their chlorophyll (Chl) *a*'s, despite a high pigment density. Here, we show, using single-molecule spectroscopy, that the FCP complexes of *Cyclotella meneghiniana* switch frequently into stable, strongly emissive states shifted 4–10 nm toward the red. A few percent of isolated FCPa complexes and ∼20% of isolated FCPb complexes, on average, were observed to populate these previously unobserved states, percentages that agree with the steady-state fluorescence spectra of FCP ensembles. Thus, the complexes use their enhanced sensitivity to static disorder to increase their light-harvesting capability in a number of ways. A disordered exciton model based on the structure of the main plant light-harvesting complex explains the red-shifted emission by strong localization of the excitation energy on a single Chl *a* pigment in the terminal emitter domain due to very specific pigment orientations. We suggest that the specific construction of FCP gives the complex a unique strategy to ensure that its light-harvesting function remains robust in the fluctuating protein environment despite limited excitonic interactions.

photosynthetic excitons | single-molecule spectroscopy | light-harvesting complex | fucoxanthin–chlorophyll protein | protein disorder

The main function of a photosynthetic light-harvesting complex is to absorb solar photons and transfer the electronic excitation energy to neighboring complexes and eventually to the reaction center, where the photoenergy is transformed into chemical energy. These processes should be efficient and robust and the machinery inexpensive. One economical consideration is the use of only a limited variety of photosynthetic pigments. Precise arrangements of the pigments in very specific environments ensure a high degree of efficiency and robustness (1–4). Specifically, spectral bandwidth and energy gradients are achieved by embedding the pigments in a protein matrix, thereby tuning the transition energies. In addition, the photosynthetic pigments are generally packed into the proteins with high density, introducing strong excitonic interactions, which lead to excited states delocalized over multiple pigments. These molecular excitons are associated with new transition energies and significantly enhance the energy transfer speed and efficiency within the complexes (5, 6). Moreover, strong excitonic interactions have a reduced sensitivity to protein conformational fluctuations, thus enhancing robustness of energy transfer. This property was recently illustrated for the main light-harvesting complex of plants, known as LHCII, showing that breaking of the strongest excitonic interactions makes the complex more susceptible to static disorder and consequently decreases its light-harvesting efficiency (7).

While the strong excitonic interactions in photosynthetic complexes may be considered a natural consequence of the complexes' high pigment densities, the light-harvesting complexes of diatoms [fucoxanthin–chlorophyll proteins (FCPs)] appear to deviate from this corollary. The major types of FCP that can be isolated from centric diatoms like *Cyclotella meneghiniana* are known as FCPa and FCPb (8). The monomeric subunits of FCPa and FCPb are physically smaller than an LHCII monomer (9, 10), and there is strong indication that FCPa and FCPb bind the same number of pigments per monomer as LHCII (11, 12), yet various experimental results have indicated that the interpigment coupling, especially between chlorophyll (Chl) *a*'s, is considerably weaker in FCP than in LHCII. First, circular dichroism spectroscopy shows a lack of Chl *a*–Chl *a* excitonic bands in the Q_y region of isolated FCPs (9, 13) as well as for FCPs in isolated thylakoids and in intact cells (14). Second, the steady-state absorption and emission spectra are blue-shifted compared with those of LHCII (8, 15). In particular, FCP's Q_y absorption band is narrower and blue-shifted and the fluorescence emission of FCPa and FCPb is shifted from ∼682 nm (as in LHCII) to ∼676 nm for FCPa and to ∼674 nm for

Significance

Photosynthetic energy transfer must remain robust within the disordered protein environment. A high degree of robustness is generally obtained using molecular exciton states, which are excited states delocalized over a few pigments. These states provide several advantages, including a reduced probability of energy trapping in unfavorable sites, which would diminish the energy transfer efficiency. This study combines single-molecule spectroscopy and quantum-mechanical simulations to explore the different strategy of the main light-harvesting complexes of diatoms to enhance robustness. In the absence of strong exciton interactions, the pigment energies are more susceptible to protein structural changes, but the complexes seem to use these fluctuations to switch frequently into low-energy states with improved light-harvesting properties.

Author contributions: T.P.J.K. and M.T.A.A. designed research; T.P.J.K., P.M., M.T.A.A., T.M., C.B., and R.v.G. performed research; C.B. contributed new reagents/analytic tools; T.P.J.K. and P.M. analyzed data; and T.P.J.K., P.M., and M.T.A.A. wrote the paper.

The authors declare no conflict of interest.

This article is a PNAS Direct Submission.

[1]To whom correspondence should be addressed. Email: tjaart.kruger@up.ac.za.

This article contains supporting information online at www.pnas.org/lookup/suppl/doi:10.1073/pnas.1714656115/-/DCSupplemental.

FCPb. Third, there is a lack of spectral evolution of the Q_y bleach upon visible time-resolved spectroscopy, showing that the Chl *a*'s (or their excitonic states) are not spectrally distinguishable (16, 17). Fourth, optically detected magnetic resonance (18) and time-resolved electron paramagnetic resonance (19) studies have shown that a significant fraction of the Chl *a* triplet state, which has a much higher yield than in LHCII, is not efficiently quenched by neighboring fucoxanthin (Fx) xanthophylls, leading to the conclusion that at least some Chl *a*'s are truly monomeric and relatively far from the surrounding Fx or the Chl *a*'s may be oriented such that the Dexter-required overlap between Chl *a* and Fx is too small for efficient triplet–triplet energy transfer to take place. The latter observation is corroborated by the fact that most of the blue-shifted Fx's appear to transfer excitation energy to the red-shifted Fx's and not directly to Chl *a* (16).

Diatoms account for more than 20% of the total oxygen production on this planet and about 50% of that in the marine environment (20, 21). Despite their important ecological role, FCP complexes have been studied in considerably less detail than the light-harvesting complexes of plants. One important reason for this is that no FCP structure has as yet been resolved. Due to the protein sequence similarity between FCPs and LHCII (22), the latter is often used as a model system in studies of FCP. LHCII, which naturally assumes a trimeric arrangement, binds eight Chl *a*, six Chl *b*, and four xanthophylls to each monomer (23). FCPa is also a trimer and when isolated from low-light acclimated cells it is composed of the very similar polypeptides fcp1–3 and a small substoichiometric fraction of fcp6, a polypeptide coded by another gene class (24). FCPb is composed of only fcp5 proteins, which are quite homologous to fcp1–3 (8, 9, 15, 25), and assemble into nonamers (10). Each monomeric subunit of FCPb binds up to eight Chl *a*, two Chl *c*, and eight Fx pigment molecules (11, 12), while FCPa is generally isolated with an identical pigment composition but one Chl *a* less per monomer, likely due to pigment loss during isolation (11). This gives a total of 18 pigments per monomer of FCPb, the same number as for an LHCII monomer. FCPa and FCPb additionally bind substoichiometric amounts of the xanthophyll-cycle carotenoids diadinoxanthin and diatoxanthin.

Protein sequence alignment has indicated that at least six Chl *a* binding sites in LHCII are conserved in FCPa/b, namely 602, 603, 610, 612, 613, and 614 (notation as in ref. 23), as well as Chl *b*609, which is likely replaced with Chl *c* in FCPa/b (11). Specifically, the transmembrane helices 1 and 3, which contain the residues that bind Chls 602, 603, 610, 612, and 613, are highly homologous in these complexes, and helix 2 and the C terminus of FCPa/b contain residues that are expected to bind Chls 614 and 609 in similar positions as in LHCII (11, 12). As a result, at least two of LHCII's terminal-emitter Chls (*a*610, *a*611, and *a*612) as well as the two other low-energy Chl dimers (*a*602–*a*603 and *a*613–*a*614) are conserved in FCPa/b. Furthermore, the two central xanthophyll binding sites, both of which occupy a lutein in LHCII, are conserved in FCP and should contain an Fx each (18).

The additional Chl *a* frequently conserved in isolated FCPb was proposed to bind at site 611 (11). Considering that LHCII's most prominent excitonic interaction takes place between Chls *a*611 and *a*612 (26), the mutual orientation and/or distance between these two pigments in FCPb should be such as to minimize excitonic coupling. Changes in the microenvironment of the pigments are then expected to enhance their excitonic coupling, which should be reflected in their spectra. Recent molecular-dynamics simulations of LHCII have shown that the Chl *a*611–Chl *a*612 cluster is subject to a significant amount of static disorder (27). Such disorder-induced spectroscopic variations are averaged out by standard bulk spectroscopy approaches but are accessible by single-molecule spectroscopy (SMS). In addition, SMS enables one to distinguish between complex-to-complex heterogeneity and spectroscopic changes occurring within a single complex on a millisecond-to-minute timescale, the timescale of slow protein dynamics (28, 29).

In this study, we present an SMS study on light-harvesting complexes of diatoms with the purpose of determining the influence of the diminished excitonic interactions on the spectroscopic and hence the light-harvesting properties of FCPa and FCPb complexes from *Cyclotella meneghiniana*. We find that these complexes display a large amount of spectroscopic heterogeneity, pointing to a strong effect of static disorder. Using SMS, we identify a light-harvesting state near 680 nm, which is consistent with the bulk steady-state fluorescence spectrum of FCPa and FCPb. The low-energy state is further characterized using SMS as well as simulations based on the LHCII structure. Relating the experimental spectra with mainly orientational changes in Chl *a*611 suggests that protein-driven dynamics of the terminal emitter Chl *a* cluster gives rise to a strong interplay between pronounced exciton localization on individual Chls and delocalization over multiple sites.

Results

Single-Molecule vs. Bulk Spectra. A single FCPa complex was found to emit mostly near 676 nm, in agreement with the bulk fluorescence spectrum (Fig. 1*A*). Taking the average of all single-molecule (SM) spectra, the bulk fluorescence spectrum was reproduced very well (Fig. 1*A*), indicating that the SM environment did not noticeably alter the conformational landscape or shifted the equilibrium between different emission states. However, a typical spectrum from a single FCPa complex was somewhat narrower than the ensemble-averaged spectra (Fig. 1*A*). The difference between the ensemble spectrum and typical SM spectrum reveals a small band centered at 682 nm (Fig. 1*C*), which indicates that the room-temperature bulk fluorescence spectrum is a convolution of a dominant ∼676-nm and a small ∼682-nm band. FCPb showed a similar relationship between its SM and ensemble fluorescence spectra, both peaking predominantly near 674 nm (Fig. 1*B*). The bulk spectrum was also somewhat broader than a typical SM spectrum (Fig. 1*B*),

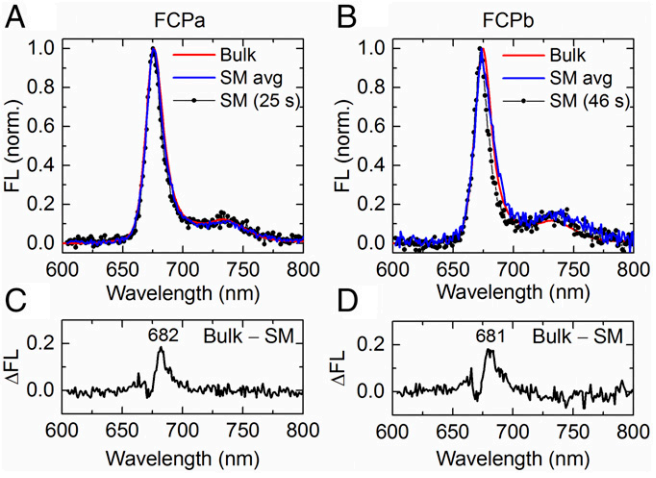

Fig. 1. Comparison between bulk and representative single-molecule (SM) fluorescence (FL) spectra. (*A*) Spectrum of a single FCPa complex, measured continuously for 25 s (SM, black); average of all FCPa SM spectra (blue) from a dataset containing 2% stable 680-nm spectra; room-temperature (RT) bulk spectrum of FCPa complexes at an OD of 0.03 (red). (*B*) Same as *A*, but for FCPb. The SM spectrum (black) was acquired during 46 s, while the population-averaged spectrum (blue) corresponds to a dataset containing 18% complexes exhibiting stable 680-nm spectra. (*C* and *D*) Difference between the bulk and SM spectrum in *A* and *B*, respectively. The peak wavelength is indicated.

the difference resulting from a low-energy emission band centered again near 680 nm (Fig. 1*D*).

The broadening toward the red of FCPb's SM population-averaged spectrum is mainly determined by the fraction of complexes exhibiting stable, narrow emission near 680 nm (e.g., Fig. 2*A*), which varied between 1% and 20%, with an average of 11%, among the five investigated data batches. For most of the datasets, the SM population-averaged spectrum of FCPb matched the bulk spectrum well (Fig. 1*D*). Inspection of the SM spectra of FCPa revealed that this complex was also capable of stable, narrow ∼680-nm emission but displayed this less frequently than FCPb: the fraction of ∼680-nm emitting complexes varied between ∼1% and ∼12% among different batches of FCPa, but the majority of batches contained only a few percent.

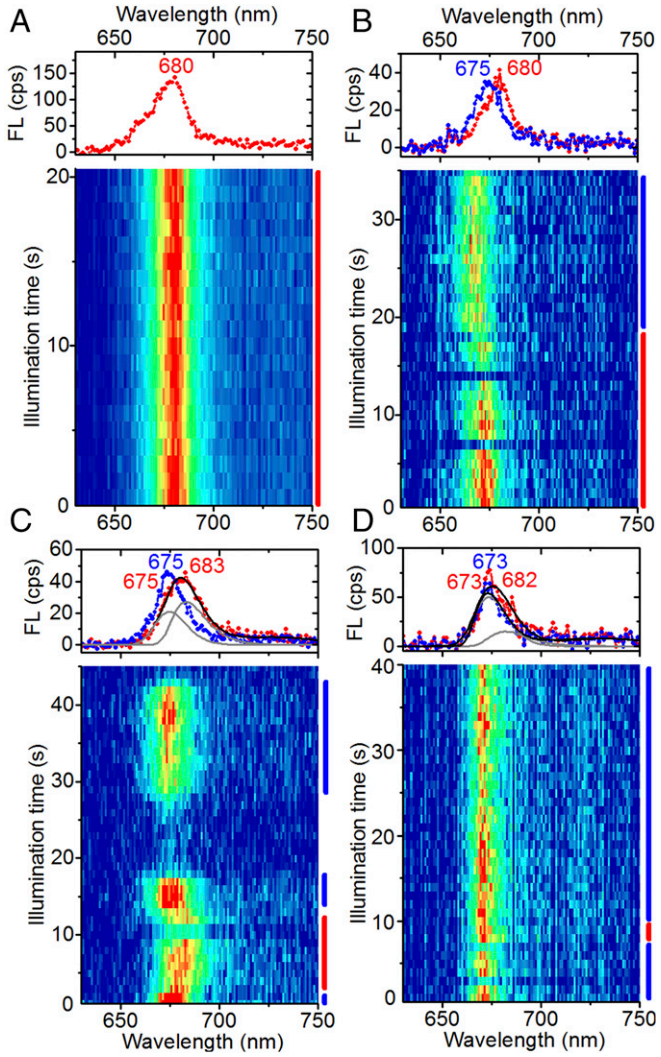

Fig. 2. Representative spectral sequences from individual FCP complexes displaying spectral dynamics near 680 nm. (*A*) Example of stable emission at 680 nm. (*B–D*) Reversible switches into emission states containing a significant fraction of emission near 680 nm. Counts were integrated into 1-s bins. Spectra on *Top* denote different stages of spectral evolution of the fluorescence (FL) emission, averaged over the times indicated by the bars with corresponding color on the *Right*. Peak positions (in nanometers) of resolved spectral bands (gray lines) are indicated on *Top*, with the color matching the corresponding spectrum. Double-band fits (thick black lines) were performed by maintaining the peak position and width of the single-band spectra (blue) in the same sequence. Large intensity variations are due to fluorescence blinking. *A* and *D* were obtained from FCPb, and *B* and *C* from FCPa.

The degree to which the varying fractions of 680-nm–emitting complexes are reflected in bulk was examined by comparing the room-temperature bulk absorption and fluorescence emission spectra of FCPa and FCPb from 14 different purifications each. For FCPa, the full width at half-maximum (FWHM) varied across 0.9 nm, which corresponds well with the variations among the different SM ensemble-averaged spectra of this complex. This result, together with the agreement between the two types of ensemble fluorescence spectra in Fig. 1*A*, indicates that the SM environment did not increase the average fraction of low-energy emission. The width of FCPb's bulk spectra varied less than its SM ensemble-averaged spectra, suggesting that, for this complex, the probability of entering the 680-nm state was sensitive to the SM environment, probably due to pigment loss and/or small conformational changes (see below). However, the agreement between the two types of ensemble spectra in Fig. 1*B* suggests that the average fraction of 680-nm emission was consistent in the two environments (SM vs. bulk). The latter conclusion is supported by our observation that the Chl *a* Q_y band of FCPb's bulk absorption spectra was on average ∼5% broader toward the red than that of FCPa, in agreement with the SM results showing a higher average probability of 680-nm emission from FCPb compared with FCPa. In a previous study, this difference between the absorption spectra of FCPa and FCPb was shown to become more pronounced at cryogenic temperatures (30).

We excluded the possibility of a population shift to low-energy emission caused by prolonged exposure of the complexes to the SM environment by inspecting two large datasets of FCPb, consisting of spectral sequences from 834 and 750 complexes, respectively. For the first dataset, the fraction of complexes exhibiting narrow 680-nm emission decreased from 24% for the first 417 complexes to 12% for the last 417 complexes, which were measured >12 h later. The second dataset showed a small variation between the fraction of ∼680-nm–emitting complexes in the first and second halves of the sample set, namely, 15% and 18%.

Properties of the 680-nm Emission States. The properties of the states characterized by emission near 680 nm were further examined by resolving the fluorescence spectral dynamics of individual FCPa and FCPb complexes under constant illumination. Out of a few thousand spectral sequences, a few examples were found where the emission switched reversibly between narrow bands peaking near 675 nm and narrow bands peaking near 680 nm (e.g., Fig. 2*B*). The quasistability of those emission states on a timescale of seconds to minutes suggests that they correspond to distinct protein conformations. Reversible switches from ∼675-nm emission to broad, red-shifted emission were more frequently observed (e.g., Fig. 2 *C* and *D*). In most instances, the blue wing of the broadened spectrum coincided with that of the preceding and succeeding ∼675-nm band (e.g., Fig. 2*D*), suggesting that the broadening originates from the appearance of an additional band near 680 nm. For cases where the blue wings do not coincide (e.g., Fig. 2*C*), a similar double-band deconvolution was possible, considering the width and peak position of the spectrum before and after the red shift. We conclude from these results that there are various quasistable conformations, each giving rise to emission near 675 nm and near 680 nm with a different amplitude ratio, and the narrow ∼680-nm spectra (Fig. 2 *A* and *B*) result from particular protein conformations where the 675-nm amplitude is small or negligible.

The amplitude ratio between the ∼675- and ∼680-nm emission bands was also affected by particular photobleaching pathways. While irreversible photobleaching mostly occurred in a single time step to the background emission level, thus indicating a fast and efficient energy trap, spectral profiles could be resolved for cases where some residual emission was left after bleaching. In most instances, the spectral profile remained the same (Fig. S1), but for a few cases there was a noticeable change, such as shown

in Fig. 3, where the ∼675-nm emission was bleached to a greater extent than the ∼680-nm emission. This example suggests that the ∼675- and ∼680-nm emissions originated from distinct sites and possibly from separate subunits of the complex, an idea that will be further explored below by simulations.

The relationship between the width and peak position of single-skewed Gaussian fits of all individual spectra was investigated next. We first selected 80 FCPb complexes exhibiting a substantial amount of emission near 680 nm. The FWHM of most spectra from these complexes was clustered around 20 nm (Fig. 4*A*), and the spectral profiles were typically very stable during the course of a measurement (Fig. 2*A*). Most of the 680-nm spectra are negatively skewed (Figs. 2*A* and 4*B*), suggesting that a small blue band (i.e., emission near 674 nm) is also present.

Performing a similar analysis on the dataset containing 18% of ∼680-nm–emitting FCPb complexes, the spectral width–peak distribution in Fig. 5*A* was obtained. To identify the most likely cluster composition, we performed Gaussian mixture modeling. A full, unshared covariance matrix for three components gives the lowest Bayesian information criterion (Fig. S2) and is therefore considered the most suitable model. Using such a model, two dominant clusters were identified (I and III), corresponding to populations with centroids at 673.8 and 680.2 nm, respectively. A third cluster shows a broad, linear correlation between the width and peak position (II). The ∼680-nm cluster corresponds to somewhat broader spectra than the ∼674-nm cluster. Considering the dataset from FCPa that contains the largest fraction of ∼680-nm emission (i.e., from ∼12% of the complexes), a similar cluster composition was identified (Fig. 5*B*). However, typical FCPa datasets contained a smaller fraction of ∼680-nm states, which rendered the ∼680-nm population too small to be identified when performing a similar statistical analysis.

The 680-nm states were characterized by strong, stable emission, pointing to a large oscillator strength. Comparison of the average intensity of spectra with peaks at or above 678 nm with those peaking below 678 nm showed that the former was consistently higher for all datasets. In our analysis, we also considered the effect of fluorescence blinking, the phenomenon of large, abrupt, reversible intensity decreases commonly observed

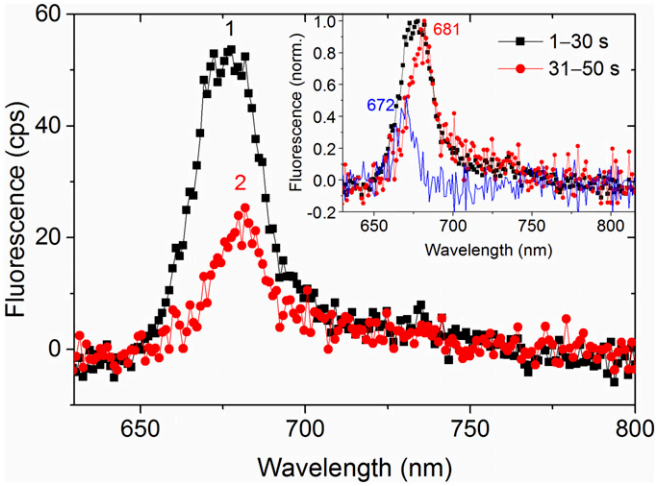

Fig. 3. Spectral dynamics during two-step bleaching of an FCPb complex. In the first step (from spectrum 1–2), the emission maximum shifted from 675 to 681 nm. (After the second step the complex was fully bleached, and the spectrum, which is indistinguishable from the background, is therefore not shown.) Spectra 1 and 2 are averaged over 30 and 20 s, respectively. The *Inset* shows the two spectra normalized, as well as the difference between the normalized spectra (blue). Peak positions (in nanometers) of the blue and red spectra are shown.

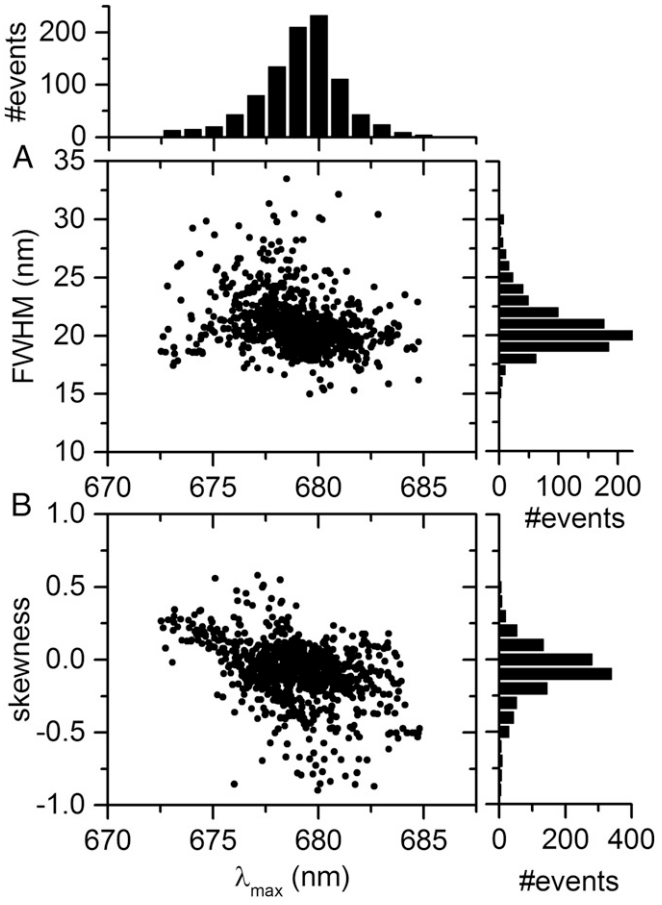

Fig. 4. Spectral properties of 680-nm emission. (*A*) Distribution of full width at half-maximum (FWHM) vs. spectral peak position (λ_{max}) of 940 spectra from 80 individually measured FCPb complexes exhibiting substantial emission near 680 nm. Each spectrum was fitted separately using single-skewed Gaussian functions. Histograms of λ_{max} and FWHM are shown on *Top* and on the *Right*, respectively, using 1-nm bins. (*B*) Skewness of single-skewed Gaussian fit vs. spectral peak position corresponding to data in *A*, using bins of 0.1 on the vertical.

from single, isolated light-harvesting complexes (31–34). Examples of long-living (∼1 s or longer) "off" events are visible in Fig. 2 *B–D*. When excluding fluorescence blinking, the intensity of the ≥678-nm spectra was on average 4% higher than that of the <678-nm spectra; when including blinking events, the difference increased to 20%. We conclude that the ∼680-nm state is not only related to a somewhat higher emission intensity when a complex is in an "on" state, but the blinking probability also decreases, suggesting these spectral states correspond to relatively stable conformational states.

Excitonic Modeling of FCP. In light of the structural homology between LHCII and FCPa/b, in particular for helices 1 and 3, which contain most of the Chl *a* binding residues, we expect the coordination of the three lowest-energy Chl *a* clusters to be highly similar for the three complexes and calculated the steady-state fluorescence spectra of FCPa/b using a disordered exciton model with the same parameters (including site energies) as for LHCII in previous simulations (7, 35). Since for LHCII the strongest excitonic coupling arises from interaction between Chls *a*611 and *a*612 (26), while FCPa/b exhibits only little excitonic coupling, we considered different ways of reducing the *a*611–*a*612 coupling. Two of the simulations serve to test the hypothesis offered in an earlier resonance Raman study (11) that Chl

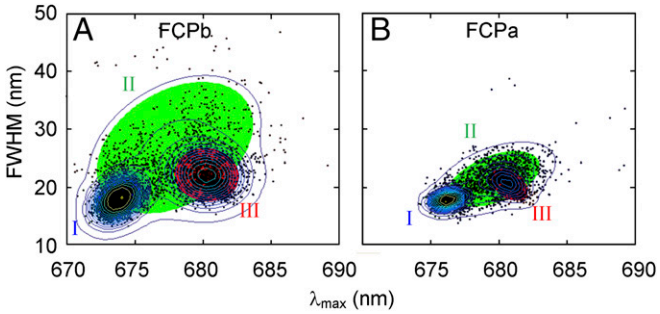

Fig. 5. Full width at half-maximum (FWHM) vs. peak position (λ_{max}) of ~4,000 spectra from individually measured (*A*) FCPb and (*B*) FCPa complexes, using single-skewed Gaussian fits. Each black dot represents the properties of a distinct fit. Only results from high-intensity spectra (>60% of the highest intensity from the sample set) are shown to limit fitting ambiguities. Three clusters were identified using Gaussian mixture modeling, and the corresponding shaded ellipses denote the 99% probability threshold for each confidence region. The overlaid contour lines are plotted in logarithmic intervals to magnify the low densities and hence match the confidence ellipses.

*a*611 is absent from FCPa and has a different, fixed orientation in FCPb. In addition, considering the sizeable orientational changes observed for Chl *a*611 in a recent molecular-dynamics study of LHCII (27), we also explored the possibility of enhanced rotational freedom of this pigment.

Fig. 6*A* shows the simulated fluorescence spectra of intact LHCII compared with LHCII with different modifications with respect to Chl *a*611. All spectra in Fig. 6*A* represent the average of 2,000 realizations, using 110-cm^{-1}-wide Gaussian site energy disorder. Removal of Chl *a*611 results in a 2.4-nm blue shift as well as a ~40% broadening of the ensemble-averaged fluorescence peak (Fig. 6*A*, red). The blue shift arises from the significantly weaker coupling in the terminal emitter domain due to the absence of *a*611, while the broadening is explained by the large spectral heterogeneity, especially into the red (Fig. 6*C*). The broadening is an overestimation, however, since the experimental bulk fluorescence spectrum of FCPa (Fig. 1*A*) is ~15% narrower than that of LHCII. This discrepancy can be explained by the large amount of excitonic coupling in our model based on LHCII's parameters, which gives rise to excitonic band splitting and subsequent broadening of the emission spectra. Since Chl *b* does not contribute to the lowest energy states in LHCII, its presence does not influence the outcome of the simulations. To realistically minimize excitonic coupling in our utilized models for FCP, constraints from an atomic structure or molecular-dynamics simulations are required.

To simulate FCPb's emission spectra, we considered three types of Chl *a*611 rotations, each of which reduced the excitonic coupling in the terminal emitter cluster. First, by randomly rotating Chl *a*611 and sampling all orientations with equal weight, using 2,000 realizations of the disorder for each orientation, a 16% broadening of the ensemble-averaged fluorescence spectrum was obtained, while the accompanying peak shifted only 0.8 nm toward the blue (Fig. 6*A*, green). In the second simulation for FCPb, we considered a particular rotation of Chl *a*611 along the polar angle that minimizes coupling with Chl *a*612 (Fig. 6*A*, magenta, and Fig. 6*E*). The results are very similar to the case of removing *a*611 (Fig. 6*A*, red, and Fig. 6*C*). In the last simulation, we chose the rotation of *a*611 along the polar angle that gives rise to the largest blue shift (3.1 nm) of the disorder-averaged fluorescence spectrum (Fig. 6*A*, blue, and Fig. 6*F*).

For each of the five cases presented in Fig. 6*A*, the relationship between the fluorescence spectral width and peak position was investigated (Fig. 6 *B*–*F*), where each data point corresponds to a different realization of the site energy disorder. The distribution corresponding to intact LHCII (Fig. 6*B*) is the narrowest and most symmetric. Of particular interest are the distributions corresponding to the removal of *a*611 in Fig. 6*C* and zero coupling between *a*611 and *a*612 in Fig. 6*E*. These distributions qualitatively reproduced the three experimental data clusters in Fig. 5: (I) a dominant, blue-shifted cluster; (II) a smaller cluster showing a linear correlation between the width and peak position; and (III) the smallest cluster corresponding to spectra with strongly red-shifted peak positions and no or little broadening, reminiscent of the single-band ~680-nm emission states (Fig. 4). For other orientations of *a*611, which correspond to stronger excitonic coupling with *a*612, clusters II and III are less prominent and the general spectral heterogeneity decreased (e.g., Fig. 6 *D* and *F*). In particular, the discrepancy between the experimental data of FCP and the simulation representing random rotation of *a*611 (Fig. 6*A*, green, and Fig. 6*D*) suggests that the pigment likely has only limited rotational freedom in its binding pocket. The most important difference between the experimental (Fig. 5) and simulated distributions of interest (Fig. 6 *C* and *E*) is the larger abundance of narrow red spectra (cluster III) obtained experimentally for FCPb. This suggests the existence of one or more protein conformational changes—not accounted for by the modeling—that promote this low-energy emission.

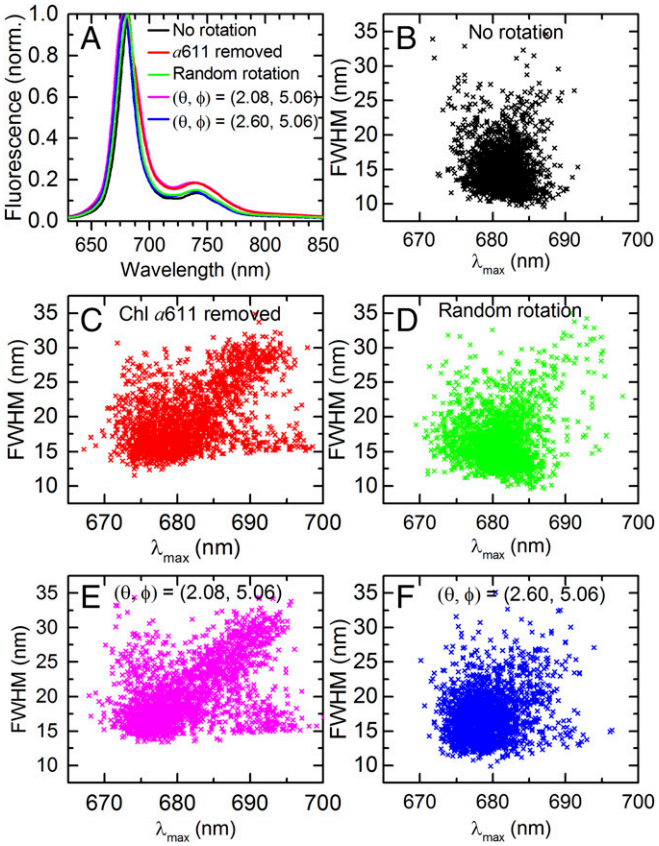

Fig. 6. Simulated spectral properties. (*A*) Modeled fluorescence spectra of LHCII with different modifications with respect to Chl *a*611, compared with the intact complex (black). Each spectrum denotes the average over 2,000 realizations of the disorder, and the green spectrum also includes the average over all orientations of *a*611. The magenta and blue spectra correspond to an orientation of the Q_y transition dipole moment of Chl *a*611 in spherical coordinates of (θ, Φ) = (2.08, 5.06) rad and (θ, Φ) = (2.6, 5.06) rad, respectively. For intact LHCII (black), this orientation is (θ, Φ) = (3.078, 5.06) rad. (*B*–*F*) Simulated distributions of FWHM vs. peak position corresponding to the color-coded spectra in *A*. Each data point represents a different realization of the disorder. Each data point in *D* represents an average over all orientations.

Discussion

Relevance of the Simulations. It is important to first establish the applicability of the simulated results in Fig. 6, which are based on the structure and site energies of plant LHCII, for a study on FCP. The highly homologous helices 1 and 3 contain the Chls that participate most to LHCII's lowest-energy exciton states responsible for the observed fluorescence emission (35). Conservation of these binding sites in FCP strongly suggests that the associated site energies cannot be significantly different in FCP. Importantly, because the site energies are relatively spread, the qualitative features of the model are relatively robust to mean site energy alterations, as shown in previous modeling of LHCII, where the spectra were reproduced with various sets of site energies (36). The main spectral differences between the fluorescence emission spectra of LHCII and FCP are therefore rather attributed to (*i*) altered pigment orientations and/or positions, which are addressed by the simulations, or (*ii*) replacement of one or two Chl *a*'s with Chl *c* in each monomeric subunit. Since the Chl *c* pigments in FCP have a ∼35-nm blue-shifted Q_y transition compared with Chl *a* (17) and transfer excitation energy to Chl *a* on an ultrafast timescale (37), they do not contribute directly to the lowest-energy excitons in FCP. In LHCII, the lowest-energy excitons are localized on Chls *a*610, *a*611, *a*612, *a*602, and *a*603 (7), and the close vicinity of xanthophylls to these sites (23) results in strong interactions between these xanthophylls and Chls *a*610, *a*611, *a*612, and *a*603 (38), while Chl *a*602 is also affected through its strong coupling with *a*603. However, since transient absorption spectra of FCP do not show evidence of energy transfer from Fx to Chl *c* (16, 17), we can rule out Chl *c*'s participation in FCP's lowest-energy exciton states.

The simulations represent the simplest model that qualitatively explains all features of the experimental data, and hence we chose not to implement further alterations to the LHCII model. For example, the simulated spectra could be blue-shifted in various ways by a combination of reduced site energies and further decrease in excitonic couplings. In our simulations for FCP, we have considered only changes with respect to *a*611 as a proof of concept, but it is likely that the specific orientation of *a*612 in FCP as well as the distance between *a*611 and *a*612 contribute to the observed effects. Modeling of Chl triplet quenching by carotenoid triplets using quantum-mechanical calculations of the central carotenoid–Chl *a* site configuration in LHCII and FCP has led to the conclusion that the Fx that couples with *a*610–*a*611–*a*612 not only has a different orientation compared with the lutein in the same binding site in LHCII, but the orientation of *a*612 in FCP is also slightly altered (19). Furthermore, molecular-dynamics simulations of LHCII have indicated that a conformational change responsible for altering the orientation of *a*611 also moved it closer to *a*612, although the *a*611–*a*612 coupling was found to be most significantly affected by the pigments' relative orientation (27).

Although it cannot be excluded that some other mechanism may account for the spectroscopic differences between LHCII and FCP, the requirements for such a model should include an explanation of all experimental results supporting FCP's weak Chl *a* excitonic coupling despite a high pigment density as well as the SMS data clusters in Figs. 4 and 5. For example, formation of hydrogen bonds (39, 40) and charge transfer states (41–43) are generally connected to spectral shifts of at least 10 nm, which are larger than the spectral changes considered in the present study. It is of note that, in a recent 77 K Stark fluorescence study on FCP aggregates, a band near 680 nm was identified, which contributed more strongly to the fluorescence and Stark fluorescence spectra of FCPb than to those of FCPa (43), in agreement with the relative abundance of 680-nm emission in the present study. In the same study, the identified ∼680-nm state exhibited no charge transfer character for the FCPa sample, while for FCPb a weak charge transfer character was attributed to this state, even though a similar 680-nm band resolved for a mixture of FCPa and FCPb complexes showed no evidence of charge transfer. We explain this discrepancy by suggesting that the 680-nm band resolved for the FCPb sample contained also a contribution of longer-wavelength emission, the latter of which originates from a state with charge transfer character. The 680-nm emission in the Stark study can then be explained by a pure excitonic model, corroborating the results in the present study.

Nature of the Red Emission States. FCP's emission near 680 nm can be divided into two types: the first type of spectrum is narrow and typically very stable (Fig. 6, cluster III), while the second is broader and quasistable (upper part of cluster II). Narrow emission near 680 nm was observed for ∼11% of the FCPb complexes, on average, and for a few percent of the FCPa complexes, while broad, red emission occurred sporadically. The simulations enable us to examine the possible origin of the 680-nm emission by considering the properties of the corresponding clusters in Fig. 6 *C* and *E*. Both types of red emission originate from strong localization of the lowest exciton, leading to an increase in the reorganization energy. Localization occurred for >96% of the realizations on one of the terminal-emitter Chls and most frequently on site 610 (Fig. S3*A*). The width of the red spectra is mainly determined by the relative contribution of the second lowest exciton state to the emission. Specifically, for the broad red spectra, the lowest two exciton levels both contribute strongly to the fluorescence, while for the narrow red spectra, the second lowest exciton state has a significantly smaller contribution to the emission. A single Gaussian fit therefore gives rise to a broad spectrum for the former but enhanced negative skewness and only little broadening for the latter (Fig. 4). A few examples of the two types of red-shifted spectra are shown in Fig. S3*B*. Since the spectral distributions were quite different for the other simulations, which represented stronger coupling between these two pigments, it is very likely that the red emission from FCP results from strong localization instead of enhanced excitonic coupling like in the case of LHCII. Spectral broadening of the low-energy emission to the blue is then caused mainly by the relative contribution of the second-lowest exciton to the emission. The simulated results corroborate the conclusion drawn from the experimental results that the protein conformation establishes the population ratio of the sites responsible for emission near 675 nm and near 680 nm.

Close inspection of Fig. 6 reveals that cluster III is larger for the case of negligible *a*611–*a*612 coupling (Fig. 6*E*) than for *a*611 loss (Fig. 6*C*), qualitatively agreeing with the experimental results of FCPb and FCPa, respectively. It is striking that our experimental data of FCPa have never shown a large 680-nm population. If cluster III variations reflected the probability of shedding *a*611 in different purifications, one would have expected FCPa to always have a large cluster III, because earlier studies have indicated that FCPa is prone to losing Chl *a*611 (11). Since this was not observed (Fig. 5*B*), we conclude that a large cluster III rather reflects the presence of *a*611, which then should have a distinctly different orientation with respect to *a*612 than for LHCII. The relatively small abundance of cluster III states for measured FCPa complexes corresponds to the simulation where *a*611 was removed (Fig. 6*C*), while the small variations between different sample batches may reflect varying fractions of complexes retaining this pigment during sample purification and further treatment or small conformational changes affecting the excited-state conformational equilibrium. Excitonic coupling is sensitive to the microenvironment of the pigments and small conformational changes are expected to influence the interplay between excitation delocalization and localization on the pigments that contribute most strongly to the emission. We anticipate cluster III to be more prominent for FCPa and FCPb complexes in their native environment where most subunits of the complexes are expected to retain this pigment.

The protein backbone of LHCII does not exhibit any specific residue as a binding site for *a*611, and this Chl is instead held in place via its central Mg by a phospholipid, which in turn interacts primarily with the protein's N terminus (23, 27). In FCPa/b, Chl *a*611 would similarly be indirectly bound to the protein and therefore more loosely bound than the other Chls (11). However, with its significantly smaller N terminus, FCPa probably loses Chl *a*611 more easily than LHCII does during protein purification. In contrast, nonameric FCPb has three trimer–trimer interfaces where Chl *a*611 will be more strongly bound and hence less easily lost. It is important to note that FCPa/b complexes in their native environment still lack excitonic interactions, as observed from thylakoid circular dichroism spectra (14, 44).

An Enhanced Light-Harvesting Function. Our simulations demonstrate the strong effect of static disorder when reducing excitonic coupling in a light-harvesting complex. LHCII's terminal emitter Chl cluster is locked into a strong excitonically coupled state, giving rise to reduced sensitivity to protein dynamics and hence enhanced robustness to the fluctuating protein environment. Strongly reduced excitonic coupling would generally be detrimental to the light-harvesting function of photosynthetic complexes, as demonstrated in a recent SMS study on the LHCII-A2 mutant (7). This mutant, which lacks both Chls *a*611 and *a*612, displays an experimental and modeled fluorescence width–peak distribution showing only cluster II but no cluster III (narrow red spectra). Furthermore, cluster II, which was explained by the same principle as in the present study (i.e., the two lowest exciton states both contributed strongly to the emission and the lowest exciton state was red-shifted due to localization), involved a significant amount of blue-shifted emission from sites other than the terminal emitter domain: (*i*) the lowest exciton state of LHCII-A2 is more delocalized than in the case of FCP, containing besides the dominant contribution from *a*610 also a strong (blue-shifted) contribution from *a*602; (*ii*) the oscillator strength of LHCII-A2's lowest exciton state is lower than for FCP because of the absence of two prominent pigments (*a*611 and *a*612), resulting in a comparatively strong contribution of the second lowest exciton state to LHCII-A2's emission. As a result of the strong blue-shifted emission always accompanying the red emission of single LHCII-A2 complexes, a sizeable fraction of excitations do not end up in the terminal emitter domain, thereby substantially reducing the efficiency of excitation energy transfer in the mutant (7).

In contrast to LHCII, FCP likely responds to its enhanced susceptibility to disorder by switching frequently into a ∼680-nm emission state, thereby retaining various light-harvesting functions normally attributed to strong excitonic interactions: (*i*) the spectral switching broadens the complex's absorption spectral window. (*ii*) It creates a steeper energy gradient within the antenna compared with conformations where ∼675 nm corresponds to the lowest energy state. A steeper gradient would be associated with faster excitation energy equilibration within the antenna. (*iii*) It favors radiative or energy transfer processes over energy losses through an increased oscillator strength, due to the likely presence of three pigments in the terminal emitter domain, as well as by reduced fluorescence blinking. (*iv*) A large degree of robustness to static disorder is maintained through the energy gap between the typical lowest energy levels in FCP (associated with ∼675-nm emission) and the reaction center (absorbing near 680 nm), as well as by possibly retaining a beneficial terminal emission site. For LHCII, it is favorable to have an excitation end up in *a*610–*a*611–*a*612, because from this domain excitations can be transferred with high efficiency to neighboring antennas. For FCP, we expect that this Chl cluster would similarly be a favorable terminal emitting site for the ∼675-nm emission. Since, in our model for FCP, the lowest exciton of the ∼680-nm emission states was localized on *a*610, *a*611, or *a*612 for >96% of the realizations of the disorder, it is likely that *a*610–*a*611–*a*612 serves as the terminal emitter cluster also for these red states. The little contribution of other pigments to FCP's low-energy emission then suggests that, in contrast to the situation for LHCII-A2, FCP's enhanced sensitivity to protein disorder does not adversely affect its light-harvesting efficiency. Instead, static disorder makes the complex switch between blue-shifted states, where most of the emission likely originates from somewhat delocalized *a*610–*a*611–*a*612, and red-shifted states, where most of the emission likely originates from strongly localized excitations in the same domain. In case *a*610–*a*611–*a*612 is not the predominant site for ∼675-nm emission, static disorder may give rise to enhanced light-harvesting efficiency by localizing the excitations in a more favorable site. Thus, the simulations suggest that FCPs can dynamically switch between a (preferential) blue-shifted emission state at ∼675 nm and a red state at ∼680 nm that may be even more efficient in light harvesting.

Conclusions

We have identified and characterized a light-harvesting state in FCP, associated with enhanced emission around 680 nm. The experimental results are qualitatively reproduced by an excitonic model based on the similarity between FCP and LHCII in terms of Chl *a* pigment composition and the protein helices containing the binding residues of these pigments, and by ensuring negligible interaction between Chls *a*611 and *a*612 or absence of *a*611. From the simulations, we conclude that (*i*) frequent switching into the 680-nm emission state results from weak Chl *a* excitonic interactions, which make the complexes energetically susceptible to static disorder; (*ii*) static disorder modulates the energy of the lowest exciton state, and hence the fluorescence spectral properties, by varying the amplitude ratio between two dominant emission bands, peaking near 675 and 680 nm, respectively; and (*iii*) the 680-nm emission is characterized by strong localization of the excitation energy in the favorable terminal emitter Chl *a* domain 610–611–612, and the exciton state responsible for emission near 675 nm likely involves the same Chl *a* domain but is more delocalized.

The simulations indicate that small orientational changes of key pigments in dense arrangements can drastically change the functionality of photosynthetic antenna complexes, an unavoidable consequence of high pigment densities in proteins, which constitute structurally fluctuating environments. Our comparison between LHCII and FCP suggests that there are at least two solutions for maintaining an efficient light-harvesting function. LHCII, like most other photosynthetic complexes, suppresses the susceptibility to disorder by means of strong excitonic interactions. FCP, on the other hand, must have a very specific construction to enable it to use the static disorder to localize excitations in sites with favorable light-harvesting properties. The 680-nm emission states represent such states. Their enhanced stability and emissivity are indicative of limited trapping of the excitation energy in thermally dissipating states, and frequent switching into the 680-nm states enlarges the spectral absorption cross-section, increases the energy gradient, and possibly localizes excitations in a beneficial site in the complex. Overcoming the adverse effects of static disorder is an important consideration for technologies such as organic and bioinspired solar cells.

Materials and Methods

Sample Preparation. FCPa and FCPb complexes were isolated from *C. meneghiniana* as described earlier (15). For the bulk measurements, the complexes were solubilized in 25 mM Tris (pH 7.4), 2 mM KCl, and 0.03% *n*-dodecyl-β,D-maltoside (β-DM). For the SMS measurements, FCPa was solubilized in an aqueous solution of 20 mM Tris (pH 8), 1 mM KCl, and 0.03% β-DM, while the FCPb complexes were found to be more stable when the buffer was replaced with 20 mM Hepes (pH 8). The complexes were diluted to a few picomolar concentration using the same buffer–salt–detergent

solution and were nonspecifically bound to a microscope coverslip glass by means of poly-L-lysine (Sigma-Aldrich). After hermetically closing the sample cell, unbound or weakly bound complexes were removed by flushing the sample cell with the same buffer–salt–detergent solution, which now contained glucose, glucose oxidase, and catalase (Sigma). The latter mixture served to scavenge oxygen in the sample cell.

Fluorescence Spectroscopy. Bulk fluorescence spectra were recorded for samples in a 0.5-cm pathlength cuvette using a Jasco fluorometer (FP-6500) and an excitation wavelength of 440 nm, as described previously (15, 45). Bulk absorption spectra were measured in a 1-cm pathlength cuvette using a Jasco V-550 spectrometer at room temperature. The SMS experimental setup described earlier (41) was used, with minor modifications. Excitation was provided by the 632.8-nm emission line of a continuous-wave He–Ne laser (JDS Uniphase), a wavelength at which the probability of carotenoid excitation is negligible. The excitation beam was passed through a Berek compensator (5540 New Focus) to obtain a near-circular polarization state. The beam was spectrally cleaned with a narrow bandpass filter (630FS10-25; Andover Corporation) and spatially cleaned using a spatial filter (KT310; Thorlabs). After sending the beam through a beam expander, the whole back aperture of the microscope objective (PlanFluor, 100×, 1.3 N.A., oil immersion; Nikon) was filled, which ensured a diffraction-limited spot at the sample plane. Complexes were identified from raster-scanned images, which were obtained by scanning the microscope stage over a 10 μm × 10-μm region of interest and directing the fluorescence photons into an avalanche photodiode (SPCM-AQR-16; Perkin-Elmer Optoelectronics). Each complex was illuminated separately and uninterruptedly for 60 s. Spectra were measured by a CCD camera (Spec10: 100BR; Princeton Instruments, Roper Scientific) after dispersion of the fluorescence by a reflective grating (HR830/800 nm; Optometrics). The spectral data were integrated in consecutive 1-s time bins. All SMS measurements were performed at 278 K and using an irradiance of 200 W/cm^2.

Data Analysis. Complexes displaying spectral blueing (i.e., spectral peaks below 670 nm) were disregarded, similarly to previous studies on complexes from plants (34, 41, 42). SM spectra were fitted with single- or double-skewed Gaussian functions in addition to a Gaussian fit of the vibrational band, as described previously (46). Ambiguity in the double Gaussian fits of the main band was reduced by using the average peak position, width, and skewness of the single-band spectra preceding and succeeding the double-band spectra. For FCPa, nine sample batches were used, and for FCPb, five sample batches. After data screening, typically >200 spectral sequences per batch were used for further analysis. Calculations were performed in Matlab R2015b (Mathworks).

Computational Methods. The modeling is based on the Hamiltonian and spectral densities used in a previous study of LHCII (7, 35). The fluorescence spectra are calculated from the steady state of the excitonic populations P_i following the kinetic equations:

$$\frac{\partial P_i}{\partial t} = \sum_j k_{ij} P_j - \Gamma_i P_i + \int d\omega W(\omega)\chi_i(\omega),$$

where k_{ij} are the population transfer rates, Γ_i are the population relaxation rates, $\chi_i(\omega)$ is the absorption spectrum of the ith exciton (see below), and $W(\omega)$ is the spectrum of the incident light. These equations can be rigorously derived from the Liouville–von Neumann equation for the reduced density matrix using second-order perturbation theory for the interaction with light, the Markovian and secular approximations, and the fact that the populations vary much slower than the optical coherences. Under these assumptions, the equations have general validity and allow calculation of excitation dynamics (47).

The excitonic absorption spectrum is given by the transition dipole strength, which can be calculated from the structure and coupling between pigments, and the calculated lineshape. The lineshape and population transfer rates are given by the bath properties, which are expressed by means of the spectral density. The absorption and fluorescence spectra are then calculated as follows (35):

$$ABS(\omega) \propto \omega \sum_i \chi_i(\omega) = \omega \sum_i |\mu_{i0}|^2 2Re \int_0^\infty d\tau e^{i(\omega-\omega_i)\tau - g_{ii}(\tau) - \frac{\Gamma_i}{2}\tau},$$

$$FL(\omega) \propto \omega^3 \sum_i P_i |\mu_{i0}|^2 2Re \int_0^\infty d\tau e^{i(\omega-\omega_i+2\lambda_i)\tau - g_{ii}^*(\tau) - \frac{\Gamma_i}{2}\tau}.$$

Here, $|\mu_{i0}|^2$ is the transition dipole moment strength for the ith exciton, ω_i is the optical transition frequency of the ith exciton, and $g_{ii}(\tau) = \sum_n |c_{in}|^4 g_n(\tau)$ is the lineshape function of the ith exciton, where c_{in} are coefficients of the site ↔ exciton basis transformation, and $|c_{in}|^2$ is the participation of the nth site in the ith exciton. The lineshape function of the nth site is given by $g_n(\tau) = \int_0^\tau dt \int_0^t dt' C_n(t')$, where $C_n(t)$ is the bath correlation function related to the spectral density $C_n(\omega)$ by Fourier transformation. We assume the same but uncorrelated bath dynamics on all of the different sites here. The reorganization energy of the ith exciton is given by $\lambda_i = \sum_n |c_{in}|^4 \lambda_n$, where $\lambda_n = 1/\pi \int_0^\infty d\omega C_n(\omega)/\omega$ is the reorganization energy of the nth site. The population transfer rates were calculated by Redfield theory, $k_{ij} = \sum_n |c_{in}|^2 |c_{jn}|^2 C_n(\omega_{ji})$, where $\omega_{ij} = (\omega_i - \lambda_i) - (\omega_j - \lambda_j)$ is the energy gap between the ith and jth exciton.

Based on the LHCII crystal structure determined by ref. 23, the excitonic coupling between pigments is calculated in the dipole–dipole approximation. For the calculated distributions and spectra, the orientation of Chl *a*611 is first changed (or it is removed) and its coupling to the other pigments is calculated. The fluorescence spectrum is then calculated for 2,000 realizations of the energetic disorder of the pigment site energies.

ACKNOWLEDGMENTS. We thank Kerstin Pieper for the bulk absorption and fluorescence measurements and Michal S. Gwizdala for critical discussions. M.T.A.A., T.P.J.K., P.M., and R.v.G. were supported by the Vrije Universiteit and by Advanced Investigator Grant 267333 (PHOTPROT) from the European Research Council (to R.v.G.). R.v.G. was further supported by the Nederlandse Organisatie voor Wetenschappelijk Onderzoek, Council of Chemical Sciences, via TOP Grant 700.58.305, and by the European Union Seventh Framework Programme Project Phonon-Assisted Processes for Energy Transfer and Sensing (GA 323901). R.v.G. gratefully acknowledges his Academy Professor grant from the Netherlands Royal Academy of Sciences. T.P.J.K. was further supported by the University of Pretoria's Research Development Program (Grant A0W679) and the Thuthuka Program of the National Research Foundation of South Africa (Grant 94107). C.B. was supported by the European Union Seventh Framework Programme Marie Curie Initial Training Network: Control of light use efficiency in plants and algae - from light to harvest (Initial Training Network-GA-2009-238017) and Deutsche Forschungsgemeinschaft Grant Bu 812/10-1. P.M. and T.M. were supported by Czech Science Foundation Grant 17-22160S.

1. Fleming GR, Schlau-Cohen GS, Amarnath K, Zaks J (2012) Design principles of photosynthetic light-harvesting. *Faraday Discuss* 155:27–41, discussion 103–114.
2. Novoderezhkin VI, van Grondelle R (2010) Physical origins and models of energy transfer in photosynthetic light-harvesting. *Phys Chem Chem Phys* 12:7352–7365.
3. Scholes GD, Fleming GR, Olaya-Castro A, van Grondelle R (2011) Lessons from nature about solar light harvesting. *Nat Chem* 3:763–774.
4. van Grondelle R, Novoderezhkin VI (2006) Energy transfer in photosynthesis: Experimental insights and quantitative models. *Phys Chem Chem Phys* 8:793–807.
5. Van Amerongen H, Valkunas L, Van Grondelle R (2000) *Photosynthetic Excitons* (World Scientific Publishing, Singapore).
6. Mirkovic T, et al. (2017) Light absorption and energy transfer in the antenna complexes of photosynthetic organisms. *Chem Rev* 117:249–293.
7. Ramanan C, et al. (2015) The role of exciton delocalization in the major photosynthetic light-harvesting antenna of plants. *Biophys J* 108:1047–1056.
8. Beer A, Gundermann K, Beckmann J, Büchel C (2006) Subunit composition and pigmentation of fucoxanthin-chlorophyll proteins in diatoms: Evidence for a subunit involved in diadinoxanthin and diatoxanthin binding. *Biochemistry* 45: 13046–13053.
9. Büchel C (2003) Fucoxanthin-chlorophyll proteins in diatoms: 18 and 19 kDa subunits assemble into different oligomeric states. *Biochemistry* 42:13027–13034.
10. Röding A, Boekema E, Büchel C (2016) The structure of FCPb, a light-harvesting complex in the diatom Cyclotella meneghiniana. *Photosynth Res* 1–9.
11. Premvardhan L, Robert B, Beer A, Büchel C (2010) Pigment organization in fucoxanthin chlorophyll a/c(2) proteins (FCP) based on resonance Raman spectroscopy and sequence analysis. *Biochim Biophys Acta* 1797:1647–1656.
12. Butkus V, et al. (2015) Coherence and population dynamics of chlorophyll excitations in FCP complex: Two-dimensional spectroscopy study. *J Chem Phys* 142:212414.
13. Joshi-Deo J, et al. (2010) Characterization of a trimeric light-harvesting complex in the diatom *Phaeodactylum tricornutum* built of FcpA and FcpE proteins. *J Exp Bot* 61: 3079–3087.
14. Szabó M, et al. (2008) Structurally flexible macro-organization of the pigment-protein complexes of the diatom *Phaeodactylum tricornutum*. *Photosynth Res* 95:237–245.
15. Gundermann K, Büchel C (2008) The fluorescence yield of the trimeric fucoxanthin-chlorophyll-protein FCPa in the diatom *Cyclotella meneghiniana* is dependent on the amount of bound diatoxanthin. *Photosynth Res* 95:229–235.

16. Gildenhoff N, et al. (2010) Oligomerization and pigmentation dependent excitation energy transfer in fucoxanthin-chlorophyll proteins. *Biochim Biophys Acta* 1797:543–549.
17. Papagiannakis E, van Stokkum IHM, Fey H, Büchel C, van Grondelle R (2005) Spectroscopic characterization of the excitation energy transfer in the fucoxanthin-chlorophyll protein of diatoms. *Photosynth Res* 86:241–250.
18. Di Valentin M, Büchel C, Giacometti GM, Carbonera D (2012) Chlorophyll triplet quenching by fucoxanthin in the fucoxanthin-chlorophyll protein from the diatom *Cyclotella meneghiniana*. *Biochem Biophys Res Commun* 427:637–641.
19. Di Valentin M, et al. (2013) Triplet-triplet energy transfer in fucoxanthin-chlorophyll protein from diatom *Cyclotella meneghiniana*: Insights into the structure of the complex. *Biochim Biophys Acta* 1827:1226–1234.
20. Falkowski PG, Barber RT, Smetacek V (1998) Biogeochemical controls and feedbacks on ocean primary production. *Science* 281:200–207.
21. Field CB, Behrenfeld MJ, Randerson JT, Falkowski P (1998) Primary production of the biosphere: Integrating terrestrial and oceanic components. *Science* 281:237–240.
22. Green BR, Kühlbrandt W (1995) Sequence conservation of light-harvesting and stress-response proteins in relation to the three-dimensional molecular structure of LHCII. *Photosynth Res* 44:139–148.
23. Liu Z, et al. (2004) Crystal structure of spinach major light-harvesting complex at 2.72 Å resolution. *Nature* 428:287–292.
24. Eppard M, Rhiel E (1998) The genes encoding light-harvesting subunits of *Cyclotella cryptica* (Bacillariophyceae) constitute a complex and heterogeneous family. *Mol Gen Genet* 260:335–345.
25. Beer A, Juhas M, Büchel C (2011) Influence of different light intensities and different iron nutrition on the photosynthetic apparatus in the diatom *Cyclotella meneghiniana* (Bacillariophyceae). *J Phycol* 47:1266–1273.
26. Novoderezhkin VI, Palacios MA, van Amerongen H, van Grondelle R (2005) Excitation dynamics in the LHCII complex of higher plants: Modeling based on the 2.72 angstrom crystal structure. *J Phys Chem B* 109:10493–10504.
27. Liguori N, Periole X, Marrink SJ, Croce R (2015) From light-harvesting to photoprotection: Structural basis of the dynamic switch of the major antenna complex of plants (LHCII). *Sci Rep* 5:15661.
28. Krüger TPJ, Novoderezhkin VI, Romero E, Van Grondelle R (2014) Photosynthetic energy transfer and charge separation in higher plants. *The Biophysics of Photosynthesis*, eds Golbeck JH, van der Est A (Springer, New York), Vol 11, pp 79–118.
29. Moerner WE (2002) A dozen years of single-molecule spectroscopy in physics, chemistry, and biophysics. *J Phys Chem B* 106:910–927.
30. Premvardhan L, Bordes L, Beer A, Büchel C, Robert B (2009) Carotenoid structures and environments in trimeric and oligomeric fucoxanthin chlorophyll a/c_2 proteins from resonance Raman spectroscopy. *J Phys Chem B* 113:12565–12574.
31. Bopp MA, Jia Y, Li L, Cogdell RJ, Hochstrasser RM (1997) Fluorescence and photobleaching dynamics of single light-harvesting complexes. *Proc Natl Acad Sci USA* 94:10630–10635.
32. Gwizdala M, Berera R, Kirilovsky D, van Grondelle R, Krüger TPJ (2016) Controlling light harvesting with light. *J Am Chem Soc* 138:11616–11622.
33. Hofkens J, et al. (2001) Triplet states as non-radiative traps in multichromophoric entities: Single molecule spectroscopy of an artificial and natural antenna system. *Spectrochim Acta A Mol Biomol Spectrosc* 57:2093–2107.
34. Krüger TPJ, et al. (2013) The specificity of controlled protein disorder in the photoprotection of plants. *Biophys J* 105:1018–1026.
35. Novoderezhkin VI, Palacios MA, van Amerongen H, van Grondelle R (2004) Energy-transfer dynamics in the LHCII complex of higher plants: Modified Redfield approach. *J Phys Chem B* 108:10363–10375.
36. Novoderezhkin V, Marin A, van Grondelle R (2011) Intra- and inter-monomeric transfers in the light harvesting LHCII complex: The Redfield-Förster picture. *Phys Chem Chem Phys* 13:17093–17103.
37. Songaila E, et al. (2013) Ultrafast energy transfer from chlorophyll c_2 to chlorophyll a in fucoxanthin-chlorophyll protein complex. *J Phys Chem Lett* 4:3590–3595.
38. Fox KF, Bricker WP, Lo C, Duffy CDP (2015) Distortions of the xanthophylls caused by interactions with neighboring pigments and the LHCII protein are crucial for studying energy transfer pathways within the complex. *J Phys Chem B* 119:15550–15560.
39. Brecht M, Studier H, Radics V, Nieder JB, Bittl R (2008) Spectral diffusion induced by proton dynamics in pigment-protein complexes. *J Am Chem Soc* 130:17487–17493.
40. Olsen JD, Sockalingum GD, Robert B, Hunter CN (1994) Modification of a hydrogen bond to a bacteriochlorophyll a molecule in the light-harvesting 1 antenna of *Rhodobacter sphaeroides*. *Proc Natl Acad Sci USA* 91:7124–7128.
41. Krüger TPJ, Novoderezhkin VI, Ilioaia C, van Grondelle R (2010) Fluorescence spectral dynamics of single LHCII trimers. *Biophys J* 98:3093–3101.
42. Krüger TPJ, Wientjes E, Croce R, van Grondelle R (2011) Conformational switching explains the intrinsic multifunctionality of plant light-harvesting complexes. *Proc Natl Acad Sci USA* 108:13516–13521.
43. Wahadoszamen M, et al. (2014) Stark fluorescence spectroscopy reveals two emitting sites in the dissipative state of FCP antennas. *Biochim Biophys Acta* 1837:193–200.
44. Ghazaryan A, Akhtar P, Garab G, Lambrev PH, Büchel C (2016) Involvement of the Lhcx protein Fcp6 of the diatom *Cyclotella meneghiniana* in the macro-organisation and structural flexibility of thylakoid membranes. *Biochim Biophys Acta* 1857:1373–1379.
45. Gundermann K, Büchel C (2012) Factors determining the fluorescence yield of fucoxanthin-chlorophyll complexes (FCP) involved in non-photochemical quenching in diatoms. *Biochim Biophys Acta* 1817:1044–1052.
46. Krüger TPJ, Ilioaia C, Johnson MP, Ruban AV, van Grondelle R (2014) Disentangling the low-energy states of the major light-harvesting complex of plants and their role in photoprotection. *Biochim Biophys Acta* 1837:1027–1038.
47. Malý P, Gruber JM, van Grondelle R, Mančal T (2016) Single molecule spectroscopy of monomeric LHCII: Experiment and theory. *Sci Rep* 6:26230.